LANGMUIR Article
Cite This: *Langmuir* 2019, 35, 9464−9473 pubs.acs.org/Langmuir

# Colloidal Gelation through Thermally Triggered Surfactant Displacement

Li-Chiun Cheng, Zachary M. Sherman, James W. Swan, and Patrick S. Doyle*

Department of Chemical Engineering, Massachusetts Institute of Technology, Cambridge, Massachusetts 02139, United States

Supporting Information

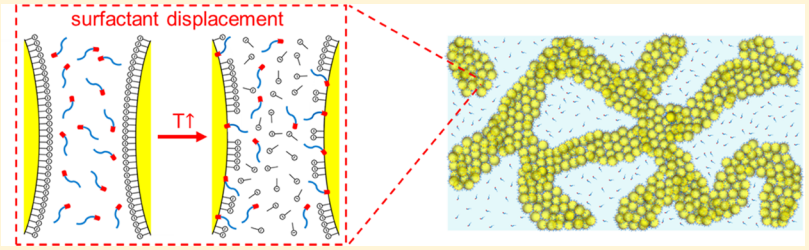


**ABSTRACT:** Colloidal systems that undergo gelation attract much attention in both fundamental studies and practical applications. Rational tuning of interparticle interactions allows researchers to precisely engineer colloidal material properties and microstructures. Here, contrary to the traditional approaches where modulating attractive interactions is the major focus, we present a platform wherein colloidal gelation is controlled by tuning repulsive interactions. By including amphiphilic oligomers in colloidal suspensions, the ionic surfactants on the colloids are replaced by the nonionic oligomer surfactants at elevated temperatures, leading to a decrease in electrostatic repulsion. The mechanism is examined by carefully characterizing the colloids, and subsequently allowing the construction of interparticle potentials to capture the material behaviors. With the thermally triggered surfactant displacement, the dispersion assembles into a macroporous viscoelastic network and the gelling mechanism is robust over a wide range of compositions, colloid sizes, and component chemistries. This stimulus-responsive gelation platform is general and offers new strategies to engineer complex viscoelastic soft materials.



## INTRODUCTION

Colloidal suspensions that undergo gelation are widely used as scaffolds in tissue engineering,[1] as carriers in drug delivery,[2] as ingredients and products in the food industry,[3,4] and as building blocks in porous material design.[5] In particular, colloidal gelation triggered by increasing temperatures has been used in various applications, such as complex material design, tissue engineering, and drug delivery. For example, our group has previously demonstrated thermally induced gelation as a bottom-up strategy for hierarchical hydrogel synthesis via three-dimensional printing.[6] Moreover, thermally gelling colloidal suspensions are also useful for biomedical and pharmaceutical applications. At room temperature, the liquid-like behavior makes the suspension easily injectable, whereas at body temperature (after injection), the colloidal self-assembly gives rise to in situ gelation, which has been utilized as scaffolds for cell culture[7] and site-specific controlled drug delivery.[8]

Tuning intercolloid interactions allow one to engineer macroscopic material properties and internal microstructures.[9] In conventional approaches, self-assembly and gelation are driven by manipulating attractions, such as electrostatic attraction,[1] depletion,[4,10,11] polymer bridging,[6,12] and dipole−dipole interaction.[13,14] On the other hand, modulating the repulsions between colloidal particles has been investigated[15−17] much less than manipulating attractions[1,4,6,10−14] as a means to drive self-assembly. One example is controlling steric repulsions to induce flocculation in dispersions of nanoparticles with grafted polymer brushes by changing the solvent quality with temperature.[15,16] Upon decreasing the temperature, stabilizing polymer brushes collapse, which leads to a decrease in the steric repulsion and an increase in affinity between polymers. Therefore, changes in interparticle repulsions are coupled to changes in attractions, making it difficult to independently control the attraction and the repulsion, and the analyses have primarily focused on the effective attraction by lumping the two interactions. Another classic example is inducing gelation by screening the electrostatic repulsion between like-charged colloids using electrolytes.[17] Adding electrolytes reduces the range of the repulsion, resulting in aggregation due to van der Waals or other attractions. However, this method to modulate interactions requires adding or removing salts, which can be challenging for material processing and manipulation. Therefore, a simple external stimulus like temperature that can modulate the interactions is highly desired.

Here, we report a stimulus-responsive gelling platform where interparticle interactions are modulated through a thermally responsive electrostatic repulsion. By including nonionic

**Received:** February 27, 2019
**Revised:** May 31, 2019
**Published:** July 12, 2019

  

DOI: 10.1021/acs.langmuir.9b00596
*Langmuir* 2019, 35, 9464−9473

thermally responsive oligomer surfactants in colloidal suspensions that are charge-stabilized by ionic surfactants, the ionic surfactants on the colloids are displaced by the nonionic oligomers at elevated temperatures. Such thermally triggered surfactant displacement results in the decrease in colloidal repulsion and hence induces the colloidal self-assembly, which is contrary to most prior studies wherein the modulation of attractive interactions has been the major focus. Our system shows rich phase behaviors and mechanical properties. We demonstrate that this gelation platform is general and robust over a wide range of compositions, colloid sizes, and component chemistry. By carefully characterizing the colloids and obtaining a mechanistic understanding of their response, we construct the interparticle potential and explain trends in material behaviors. We also show that our gelling system is in good agreement with well-established theories in the literature and therefore can be predictably extended to other systems.

## MATERIALS AND METHODS

**Materials.** Polydimethylsiloxane (PDMS, viscosity = 5 cSt), sodium dodecyl sulfate (SDS), sodium dodecylbenzenesulfonate (SDBS), cetrimonium bromide (CTAB), Tween 20, poly(ethylene glycol) methacrylate (PEGMA, $M_n \approx 360$ g mol$^{-1}$), poly(ethylene glycol) methyl ether (PEGME, $M_n \approx 350$ g mol$^{-1}$), poly(ethylene glycol) (PEG, $M_n \approx 300$ g mol$^{-1}$), and Nile Red were purchased from Sigma-Aldrich. Poly(ethylene glycol) acrylate (PEGA, $M_n \approx 400$ g mol$^{-1}$) was purchased from Monomer-Polymer and Dajac Labs. Unmodified latex polystyrene (PS) nanoparticles with particle diameter $D$ = 58 nm (aqueous suspension with the concentration of 10% w/v) were purchased from Magsphere, Inc., and the water was removed by placing the solution in an oven at $T$ = 50 °C. All chemicals were used without further purification.

**Nanoemulsion Synthesis.** The oil-in-water nanoemulsions studied in this work contained PDMS droplets (with diameter $D$ and volume fraction $\phi$) suspended in an aqueous continuous phase of oligomers (with volume fractions $P$) and surfactants. The total concentration of the surfactant was 0.175 M. The canonical system was composed of oil droplets ($D$ = 50 nm and $\phi$ = 0.30) suspended in a continuous phase containing SDS and PEGMA with $P$ = 0.33. To synthesize the nanoemulsion, a pre-emulsion was first prepared by adding PDMS to a premixed continuous phase and agitating with magnetic stirring at a speed of 600 rpm for 15 min to ensure there was no visually observed bulk phase separation. The premixed continuous phase consisted of deionized water, surfactants at a concentration of 0.175 M, and oligomers with $P$. The pre-emulsion was passed through a high-pressure homogenizer (EmulsiFlex-C3, Avestin) at a homogenizing pressure of 18 kpsi to form the nanoemulsion. The homogenization was conducted for various numbers of passes, N, depending on the target droplet size (Supporting Information Section S1). For example, $N$ = 12 for the canonical nanoemulsion with $D$ = 50 nm. A heat exchanger was used at the outlet of the homogenizer with 4 °C water circulating, and the emulsion was subsequently cooled to 4 °C in the refrigerator between each pass to prevent thermally induced gelation and oligomer adsorption during the homogenization. The droplet size and the polydispersity were measured using dynamic light scattering (90Plus PALS, Brookhaven Instruments) after diluting the sample to $\phi$ = 0.002. All nanoemulsions have a size polydispersity of 0.22 ± 0.02 in this work.

**Rheological Characterization.** All rheological properties were measured by using a stress-controlled rheometer (DHR-3, TA instrument) equipped with a 1° 60 mm aluminum upper cone and a temperature-controlled Peltier lower plate. To minimize evaporation, a deionized water-wetted solvent trap was used, and a few drops of deionized water were added on top of the aluminum cone. For each measurement, a preshear step was performed by applying a constant rotation at a speed of 10 rad s$^{-1}$ for 30 s and the measurement started after a 60 s period where the nanoemulsion remained quiescent at 20.0 °C. Freshly loaded nanoemulsion was used for each measurement to avoid the effect of thermal history.[12]

Small-amplitude oscillatory shear (SAOS) at a shear strain $\gamma$ = 0.05% was performed to conduct the frequency-sweep measurements and temperature-jump experiments. The frequency-sweep measurements at various temperatures, $T$, were conducted with angular frequency $\omega$ = 1 to 200 rad s$^{-1}$, and dynamic linear viscoelasticity was obtained. Before each measurement, the temperature was kept at $T$ for 10 min to reach a quasi-equilibrium (Supporting Information Section S2). For the nanoemulsion with $P$ = 0.33 and $\phi$ = 0.10, $\gamma$ = 0.03% was applied to stay in the linear regime. Temperature-jump experiments were performed by a three-stage time-sweep SAOS measurement at $T$ = 20 or 55 °C with $\omega$ = 20 rad s$^{-1}$. The measurements started with $T$ = 20 °C for 5 min, and the temperature was jumped to 55 °C for 10 min. The temperature was either maintained at 55 °C or decreased to 20 °C in the third stage. Different yield stresses were performed at the beginning of the third stage for 1 min (see Supporting Information Section S2.2 for more details).

Large-amplitude oscillatory shear (LAOS) was performed to determine the strain at the limit of linearity, $\gamma_L$. Before the measurement, the nanoemulsion was kept at $T = T_{gel}$ + 25 °C for 10 min. LAOS was then carried out over a range of shear strain values of $\gamma$ = 0.001−5% at an angular frequency of 20 rad s$^{-1}$. $\gamma_L$ is then defined as the shear strain where the viscoelastic moduli start to deviate from the linear region. Following the method by Shih et al.,[18] $\gamma_L$ is experimentally chosen as the point where $G'$ deviates more than 5% from the plateau in the linear regime.

**Isothermal Titration Calorimetry (ITC).** ITC measurements were performed using TA Instrument Nano ITC calorimetry. The experimental procedure and the data analysis followed a methodology similar to the work on study of the adsorption of proteins onto nanoparticles[19] (see Supporting Information Section S3 for more data analysis details). Before each measurement, the reference cell was filled with fresh aqueous SDS solution at a concentration of 5.3 mM and the sample cell was filled with the fresh nanoemulsion with $\phi$ = 0.001 suspended in an aqueous continuous phase containing free SDS at a concentration of 5.3 mM. The SDS concentration was chosen to be well below the critical micelle concentrations across the experimental temperature window.[20] During the measurement, 25 injections of 10 $\mu$L of PEGMA aqueous solution ($P$ = 0.00748 and [SDS] = 5.3 mM) were titrated from a syringe into the sample cell with a continuous stirring at a speed of 200 rpm. Each injection was separated with a 300 s interval to ensure equilibrium was reached (Supporting Information Section S3.2). The blank tests were conducted by titrating PEGMA aqueous solution into the sample cell filled with an aqueous solution of 5.3 mM SDS. The heat data was then subtracted from the data of the blank test, and the background-corrected data was used for the subsequent analysis (Supporting Information Section S3.3).

**ζ-Potential.** ζ-Potentials of the nanoemulsion droplets were measured by a Brookhaven Instruments 90Plus PALS zetasizer. The sample nanoemulsion was with $\phi$ = 0.001 suspended in an aqueous continuous phase containing free SDS at a concentration of 5.3 mM and PEGMA at a volume fraction of 0.00187. Before each measurement, the temperature was raised to the target temperature for 10 min. Fresh nanoemulsion was loaded for each measurement.

**Confocal Microscopy.** The microstructures of the nanoemulsion at $T$ = 20.0 and 55.0 °C were captured using a confocal laser scanning microscope (LSM 700, Zeiss) equipped with a 20× air-immersion objective. The temperature was controlled using a heating stage (Heating Insert P S1, Zeiss) with a temperature controller (TempModule S1, Zeiss). Before the nanoemulsion synthesis, PDMS was fluorescently labeled by predissolving the lipophilic dye, Nile Red (excitation/emission wavelength = 550/626 nm) at a concentration of 0.05 mg mL$^{-1}$. To image the microstructure, 150 $\mu$L of the fluorescently labeled nanoemulsion was loaded into a glass chamber (Lab-Tek 155411, Thermo Fisher Scientific) with a coverlid. The chamber was mounted on the heating stage equipped on the



DOI: 10.1021/acs.langmuir.9b00596
Langmuir 2019, 35, 9464−9473

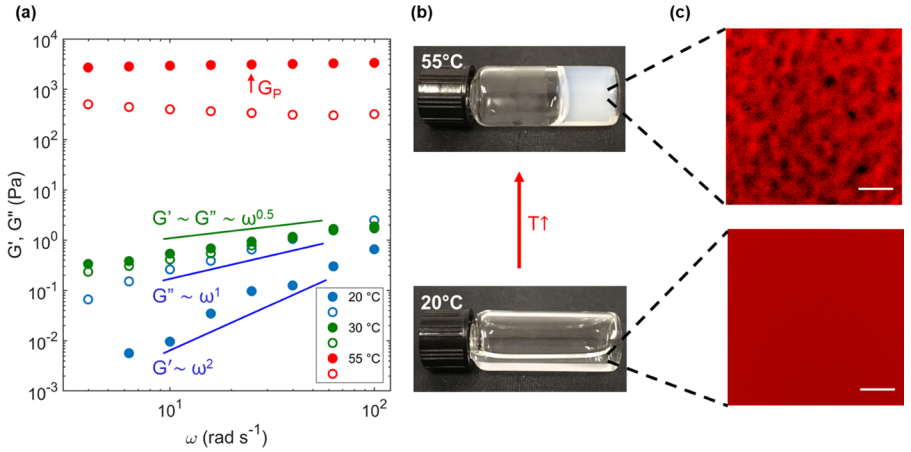


**Figure 1.** Thermally triggered gelling behavior of the model nanoemulsion system. The canonical system contains PDMS droplets (diameter $D$ = 50 nm, volume fraction $\phi$ = 0.30) suspended in an aqueous continuous phase containing PEGMA (volume fraction $P$ = 0.33) and SDS. (a) Linear viscoelasticity, storage modulus $G'$ (closed symbols), and loss modulus $G''$ (open symbols) of the nanoemulsion at various temperatures. At $T$ = 20 °C, the nanoemulsion is liquidlike. At $T$ = 30 °C, the nanoemulsion undergoes a sol−gel transition where $G'(\omega) \sim G''(\omega) \sim \omega^{0.5}$ gives the gelation temperature $T_{gel}$ = 30 °C. At $T$ = 55 °C, the nanoemulsion is solidlike where $G'(\omega)$ is nearly independent of $\omega$. (b) Photographs of the nanoemulsion taken after 10 min at $T$ = 20 and 55 °C. (c) Microstructures of the nanoemulsion at $T$ = 20 and 55 °C captured using confocal microscopy. Oil droplets were fluorescently labeled with a lipophilic dye, Nile Red, before the nanoemulsion synthesis. At $T$ = 20 °C, the droplets are homogeneously suspended in the continuous phase. At $T$ = 55 °C, the nanoemulsion droplets self-assemble into a spanning network of droplet-rich domains characteristic of arrested phase separation. Scale bars = 10 $\mu$m.

microscope. Before the imaging, the temperature was increased to the target temperature and was kept for 10 min.

## RESULTS AND DISCUSSION

**Thermally Gelling Nanoemulsions.** In this work, we used nanoemulsions as a model colloidal system, although we will show that the colloidal gelation can be applied to other colloidal suspensions. Nanoemulsions are liquid−liquid dispersions where the droplet size is ∼100 nm. Because of their stability, large interfacial surface area, and ease of synthesis, there is emerging interest for fundamental studies and practical applications of nanoemulsions in various fields.[21] Additionally, due to flexibility in the formulation, interdroplet interactions are easily tuned, making nanoemulsions a powerful model system to study aspects of soft matter physics, such as self-assembly,[22] gelation,[12] and suspension rheology.[23] Here, the canonical system consists of polydimethylsiloxane (PDMS) droplets with a volume fraction $\phi$ = 0.30 dispersed in an aqueous phase containing poly(ethylene glycol) methacrylate (PEGMA) with a volume fraction $P$ = 0.33. The droplets have a diameter of $D$ = 50 nm and are stabilized by the ionic surfactant sodium dodecyl sulfate (SDS). The nanoemulsion is liquid at room temperature but transforms into a solidlike gel upon increasing temperature. We studied this transition using small-amplitude oscillatory shear to measure the linear viscoelastic storage modulus $G'$ and loss modulus $G''$. In Figure 1a, we show the viscoelastic response over a range of angular frequencies, $\omega$. The material shows liquidlike behavior, where $G'(\omega) \sim \omega^2$ and $G''(\omega) \sim \omega$ at room temperature.[16] Upon heating, $G'(\omega)$ and $G''(\omega)$ grow and their frequency dependence changes. $G'$ and $G''$ have the same scaling with $\omega$, $G'(\omega) \approx G''(\omega) \sim \omega^{0.5}$, at the critical gelation temperature $T_{gel}$ = 30 °C. According to the classic work by Chambon and Winter,[24,25] at the critical gelation point, $G'(\omega)$ and $G''(\omega)$ have the same power law behavior where $G' \sim G'' \sim \omega^n$ and $n$ is the relaxation exponent. At this critical gel point, the colloidal system forms a sample-spanning gel network. For our canonical formulation, $T$ = 30 °C corresponds to the Chambon−Winter critical condition and this criterion is used to define the gelation temperature (Figure 1a). Moreover, in our system, $n$ is ≈0.5, which indicates the formation of a percolated gel or a pretransitional glass phase.[26,27]

Further heating the nanoemulsion leads to a dramatic increase in the elasticity, and the increase becomes limited above $T_{gel}$ + 20 °C (Supporting Information Section S2). In this high-temperature regime, $G'(\omega) > G''(\omega)$ and $G'(\omega)$ is nearly independent of frequency with a plateau modulus, $G_P$. The nanoemulsion system shows a remarkable sol−gel transition as the elasticity increases by nearly 4 orders of magnitude and the nanoemulsion transforms from a transparent liquid to a turbid, solidlike material shown in Figure 1b. The turbidity indicates the formation of droplet aggregates. To further probe the gel microstructure, confocal microscopy was used to visualize the gel network, as shown in Figure 1c. The microstructure of our nanoemulsion gel is a spanning network of colloid-rich and colloid-lean domains, similar to networks observed from arrested phase separation of other attraction-driven colloidal gels.[10,11] Interestingly, the nanoemulsion gel can re-enter the liquid state with sufficient cooling and moderate shearing (see Supporting Information Section S2.2).

**Mechanism of Colloidal Gelation.** We then investigated the gelling mechanism, and a schematic of the proposed mechanism is presented in Figure 2a. At room temperature, the SDS-stabilized droplets homogeneously disperse in the continuous phase containing PEGMA. However, PEGMA molecules provide a strong depletion interaction at ≈30 kT (for $P$ = 0.33 and $D$ = 50 nm), and because the dispersion is homogeneous at room temperature, we assumed this attraction is overcome by a strong electrostatic repulsion from the charged SDS on the droplets. This hypothesis was confirmed by measuring the $\zeta$-potential of droplets, $\zeta$, shown in Figure 2b and by calculating the corresponding repulsion strength (≈35 kT, details in later discussion). However, as temperature increases, the nanoemulsion suspension gels. We hypothesized that the gelation results from a decrease in repulsion through displacement of the ionic surfactant on the droplet surface and



DOI: 10.1021/acs.langmuir.9b00596
Langmuir 2019, 35, 9464−9473

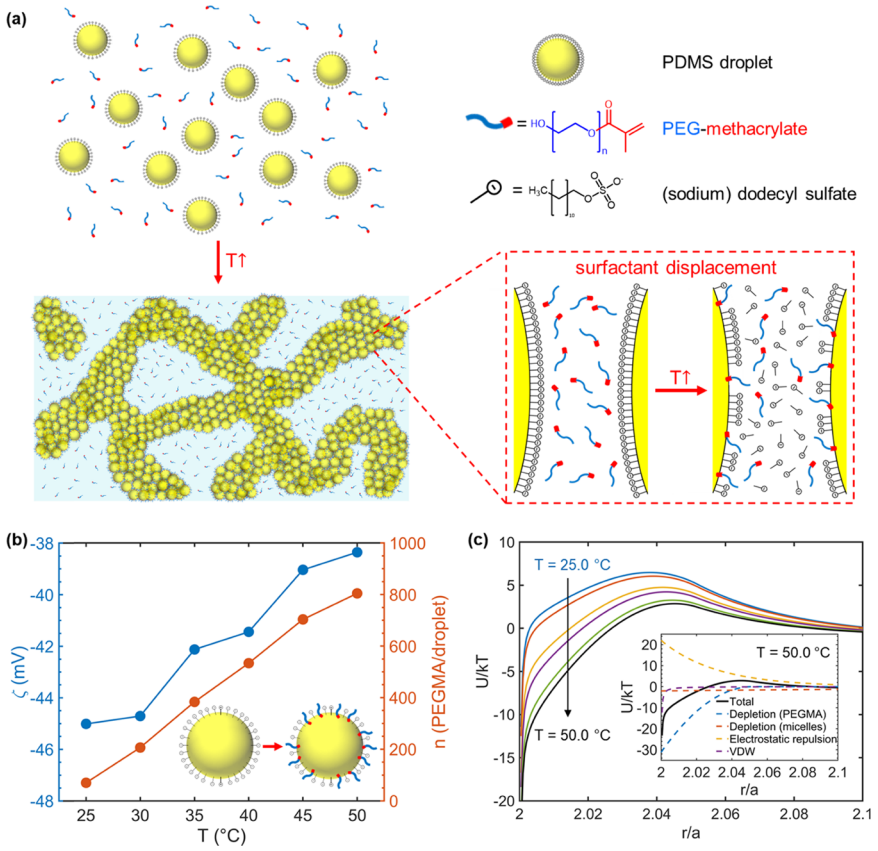


**Figure 2.** Thermally triggered surfactant displacement mechanism. (a) Schematic of the proposed gelling mechanism. At elevated temperatures, the methacrylate groups of PEGMA partition into the oil/water interface and displace the SDS. The displacement of SDS decreases the repulsive interaction between colloids. The excess PEGMA in the continuous phase provides a significant depletion attraction, and together with the depletion from SDS micelles and the van der Waals interactions, the droplets self-assemble into gels. Contributions to the interaction potential as a function of distance are shown in the inset of (c). (b) Temperature-dependent $\zeta$-potential, $\zeta$ (blue symbols, left $y$-axis), and the number of PEGMA adsorbed per droplet, $n$ (red symbols, right $y$-axis). As temperature increases, $|\zeta|$ decreases while $n$ increases, supporting our hypothesis that PEGMA replaces SDS on the droplet, which decreases the surface charge and electrostatic repulsion. (c) Interaction potential at rising temperatures, as a function of droplet center-to-center distance $r$ scaled by the droplet radius $a$. The inset shows the contributions to the potential at $T$ = 50.0 °C from depletion from PEGMA, depletion from SDS micelles, electrostatic repulsion, and van der Waals (vdW) interaction. As temperature increases, the repulsive barrier decreases and the nanoemulsions can overcome the barrier to self-assemble into a gel.

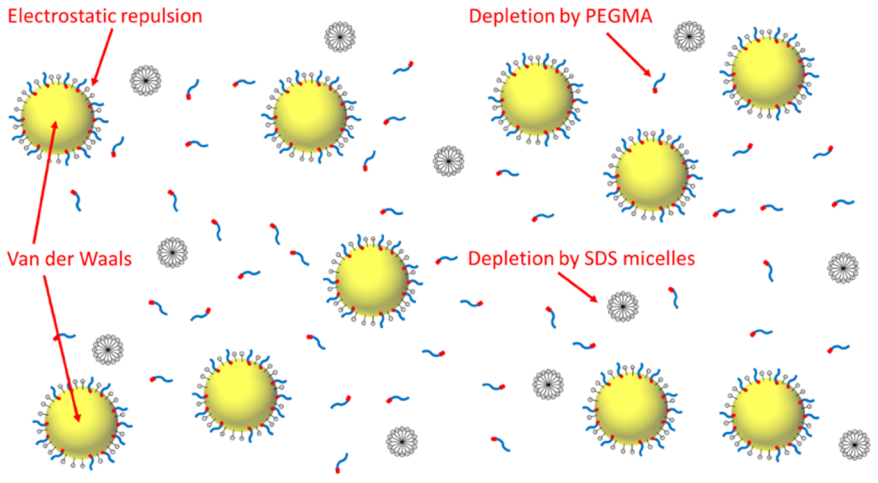


**Figure 3.** Schematic diagram of the system used for estimating the interactive potentials. A total of four interactions were considered: electrostatic repulsions, depletion by PEGMA, depletion by SDS micelles, and van der Waals interaction.

the strong depletion force from the excess PEGMA molecules in solution. To validate the hypothesis, we measured $\zeta$ at elevated temperatures. We found that the magnitude of $\zeta$ decreases with temperature, as shown in Figure 2b, whereas $\zeta$ is unchanged without PEGMA (Supporting Information Section S3), indicating desorption of SDS[17,28] in the presence of PEGMA. Isothermal titration calorimetry (ITC) was performed to further probe the adsorption of PEGMA. We



DOI: 10.1021/acs.langmuir.9b00596
Langmuir 2019, 35, 9464−9473

obtained the quantitative adsorption behavior at elevated temperature by analyzing the heat associated with the adsorbing reaction (Supporting Information Section S3). As shown in Figure 2b, the number of PEGMA adsorbed per droplet, $n$, increases with temperature. The trends of $\zeta(T)$ and $n(T)$ support the hypothesis of a thermally triggered SDS replacement by PEGMA on the nanoemulsion surface. Upon heating, the methacrylate group on PEGMA becomes increasingly hydrophobic and partitions into the oil/water interface. The proposed mechanism is further supported by ITC results where the PEGMA adsorption is an entropy-driven process (endothermic adsorption): the dehydration of the methacrylate groups frees the water molecules and results in an increase in translational entropy.[19] Finally, we showed that $\zeta$ and $n$ are quantitatively correlated using the Grahame equation[28] where the surface potential is estimated from the charge density (Supporting Information Section S3).

**Estimation of Interactive Potentials.** The overall pairwise interaction between droplets has contributions from depletion attraction arising from both PEGMA molecules and SDS micelles in solution, electrostatic repulsion, and van der Waals interactions shown in Figure 2c. The interactions from each contribution are depicted in Figure 3. We can estimate each contribution to the pair potential to better understand the gelation. Note that in our system, PEGMA has two roles: the nonadsorbing PEGMA molecules ($\sim 10^6$ per droplet) in the continuous phase provide the depletion interaction, and the adsorbed PEGMA molecules ($\sim 10^3$ per droplet) on the droplets lead to the decrease in electrostatic repulsion by displacing SDS.

**Electrostatic Repulsion.** To estimate the electrostatic repulsion, $U_{elec}$, Yukawa repulsion is considered as followed[17,28]

$$U_{elec} = \varepsilon_{elec}\frac{2a}{r}\,e^{-\kappa(r-2a)} \tag{1}$$

where $a$ is the droplet radius and $r$ is the droplet center-to-center distance. $\kappa^{-1}$ is the Debye length, and is estimated as followed

$$\kappa^{-1} = \sqrt{\frac{\varepsilon_o \varepsilon_r kT}{1000e^2 N_A \sum z_i^2 M_i}} \tag{2}$$

where $\varepsilon_o$ is the electric permeability of free space, $k$ is the Boltzmann constant, $T$ is the absolute temperature, $e$ is the elementary charge, $N_A$ is Avogadro's number, $z$ is the charge number, and $M$ is the molar concentration. $\varepsilon_r$ is the dielectric constant of the continuous phase, which is calculated by considering the dielectric constants of water[29] and PEGMA. The dielectric constant of PEGMA is estimated from the dielectric constant of PEG backbone.[30] $\varepsilon_r$ is then calculated using the mixing rule, for which the deviation from the measured value is shown to be negligible at the high PEG concentration regime such as the case in our system.[31] Table 1 lists $\varepsilon_r$ of PEG, water, and the continuous phase using the mixing rule and the resulting $\kappa^{-1}$ from eq 2.

The strength of the electrostatic repulsion, $\varepsilon_{elec}$, is estimated from[17,28]

$$\varepsilon_{elec} = 32\pi\varepsilon_o\varepsilon_r\left(\frac{kT}{ze}\right)^2 a \tanh^2\left(\frac{ze\xi}{4kT}\right) \tag{3}$$

**Table 1. Dielectric Constants of PEG, Water, and the Continuous Phase, and the Corresponding Debye Length $\kappa^{-1}$ Using Equation 2**

| $T$ (°C) | $\varepsilon_{r,PEG}$ | $\varepsilon_{r,water}$ | $\varepsilon_r$ | $\kappa^{-1}$ (nm) |
|---|---|---|---|---|
| 25 | 19.05 | 78.30 | 58.75 | 0.809 |
| 30 | 18.30 | 76.55 | 57.32 | 0.806 |
| 35 | 17.55 | 74.83 | 55.93 | 0.802 |
| 40 | 16.80 | 73.15 | 54.56 | 0.799 |
| 45 | 16.05 | 71.51 | 53.21 | 0.795 |
| 50 | 15.30 | 69.91 | 51.89 | 0.791 |

which is obtained from the Gouy−Chapman solution to the Poisson−Boltzmann equation with the superposition assumption and the Derjaguin approximation.

**PEGMA Depletion.** The PEGMA depletion is the dominant attraction due to the high concentration. In fact, the depletion interaction between nanosized colloids has been widely studied by both experiments[32−34] and simulations.[35,36] To estimate the depletion from nonadsorbing PEGMA, the Asakura−Oosawa potential is used[37,38]

$$U_{dep} = -\frac{\varepsilon_{dep}(a+\delta_P)^3}{\delta_P^2\left(\frac{3a}{2}+\delta_P\right)}\left[1 - \frac{3r}{4(a+\delta_P)} + \frac{1}{16}\left(\frac{r}{a+\delta_P}\right)^3\right] \tag{4}$$

when $2a \le r \le 2(a+\delta_P)$. Here, we also assumed that PEGMA is an ideal polymer. Therefore, an additional configurational entropy from the depletants contributes to the depletion strength, $\varepsilon_{dep}$, and the interaction range, $\delta_P$.[38] $\varepsilon_{dep}$ and $\delta_P$ are then calculated as

$$\varepsilon_{dep} = \phi_P\frac{a}{R_g}3\ln 2 \tag{5}$$

$$\delta = \sqrt{2\ln 2}\,R_g \tag{6}$$

where $\phi_P$ is the depletant volume fraction and $R_g$ is the radius of gyration of the depletant.

For the estimation, we simply assumed that the morphology of the PEGMA is independent of the temperature. Moreover, the ITC result from Figure 2b shows that the number of PEGMA adsorbed per droplet is $\sim O(10^3)$ whereas the total number of PEGMA molecules in the system per droplet is $\sim O(10^6)$, suggesting a negligible change in PEGMA concentration in solution as $T$ increases. Therefore, the PEGMA depletion presumably remains constant across the temperature window (25−50 °C).

**SDS Micelle Depletion.** Depletion by SDS micelles is also estimated using the Asakura−Oosawa potential. By assuming that the micelles behave like hard spheres, the micelle depletion is calculated as follows[38−40]

$$U_{dep} = -(\xi C_m kT)\left(\frac{\pi a}{2}(d_{m,eff} - (r-2a))^2\right) \tag{7}$$

when $2a \le r \le 2a + d_{m,eff}$ and

$$\xi = \frac{1 + \phi_{m,eff} + \phi_{m,eff}^2 - \phi_{m,eff}^3}{(1-\phi_{m,eff})^3} \tag{8}$$

where $\phi_{m,eff}$ is the effective volume fraction of micelles by considering the Debye layer[23] and is calculated as



DOI: 10.1021/acs.langmuir.9b00596
Langmuir 2019, 35, 9464−9473

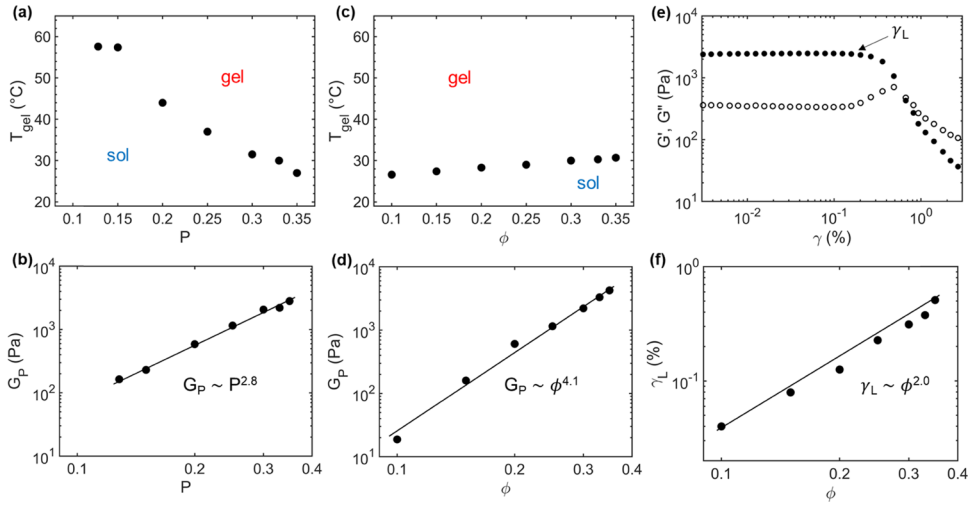


**Figure 4.** Gelling mechanism is robust over a wide range of compositions. (a) $T_{gel}$ as a function of PEGMA volume fraction in the continuous phase, $P$. (b) $G_P$ as a function of $P$ showing a power-law dependence of $G_P \sim P^{2.8}$. Nanoemulsions in (a) and (b) are composed of PDMS droplet with $D = 50 \pm 1$ nm and a volume fraction of $\phi = 0.30$. (c) $T_{gel}$ as a function of $\phi$. Because the bulk SDS concentration decreases with increasing $\phi$, $T_{gel}$ decreases slightly due to weaker micelle depletion attraction. (d) $G_P$ as a function of $\phi$, showing a power-law dependence of $G_P \sim \phi^{4.1}$. Nanoemulsions in (c) and (d) are composed of PDMS droplet with $D = 50 \pm 1$ nm dispersed in the continuous phase with $P = 0.33$. (e) $G'$ and $G''$ as a function of the shear strain, $\gamma$. The strain at the limit of linearity, $\gamma_L$, is the strain at which $G'$ and $G''$ begin to change with $\gamma$. The nanoemulsion used here is composed of PDMS droplet with $D = 50$ nm and $\phi = 0.30$ suspended in the continuous phase with $P = 0.33$. (f), $\gamma_L$ as a function of $\phi$, showing a power-law dependence of $G_P \sim \gamma^{2.0}$.

$$\phi_{m,eff} = \frac{4\pi}{3}\left(\frac{d_{m,eff}}{2}\right)^3 C_m = \frac{4\pi}{3}\left(\frac{d_m + 2\kappa^{-1}}{2}\right)^3 C_m \quad (9)$$

$C_m$ is the concentration of the micelle and is calculated as

$$C_m = \frac{(C_o - C_{ads} - C_{CMC})N_A}{N_{agg}} \quad (10)$$

where $C_o$ is the total concentration of SDS, $C_{ads}$ is the concentration of SDS adsorbed on the droplets, $C_{CMC}$ is the critical micelle concentration (≈8 mM),[20,41,42] and $N_{agg}$ is the aggregation number of micelle (≈60).[20,41,42] For the estimation, we assume that the morphology of the micelles is independent of the temperature.

**Van der Waals Interaction.** Van der Waals interaction is estimated as follows[28]

$$U_{vdW} = \frac{-Aa}{12(r - 2a)} \quad (11)$$

by assuming a uniform droplet size, and the Derjaguin approximation is used. Here, $A = 3.3 \times 10^{-22}$ J is the Hamaker constant of PDMS−water−PDMS.[43,44]

**Overall Pairwise Interaction.** As shown in Figure 2c, increasing temperature leads to a decrease in the repulsive barrier and the system can more easily overcome this energetic barrier to self-assemble and undergo gelation. We acknowledge that the quantitative behavior of the potentials may not be precisely captured, but the estimations provide mechanistic insight to explain trends in material microstructures and rheological properties (shown in Figure 4 and Supporting Information Section S2).

**Effect of Material Composition.** Controlled gelation via this mechanism is general and robust over a wide range of compositions, colloid sizes, and component chemistry. We tested the gelling mechanism by investigating the material phase behavior ($T_{gel}$) and gel elasticity ($G_P$) over a wide range of formulations. First, we demonstrated that nanoemulsion gelation can be robustly controlled over a wide range of compositions $P$ shown in Figure 4a,b and $\phi$ shown in Figure 4c,d. We found that $T_{gel}$ decreases significantly with $P$ for $0.13 \leq P \leq 0.35$, indicating the gelation is more easily induced when more depletants are present. In contrast, $T_{gel}$ increases mildly with $\phi$ for $0.1 \leq \phi \leq 0.35$, which is contrary to common colloidal systems where larger $\phi$ facilitates the gelation. We believe that such a trend with respect to $\phi$ results from a decrease in SDS micelles and electrostatic screening.[39] To validate this postulate, we studied the effect of [SDS] on the properties of the nanoemulsion gels (Supporting Information Section S2.3). The results are consistent with our predicted trend wherein a decrease in the total [SDS] leads to an increase in the gelation temperature and a decrease in the gel strength. For data in Figure 4, we kept the total [SDS] = 0.175 M constant so more SDS remains in the continuous phase with smaller $\phi$, leading to stronger micelle depletion and electrostatic screening.

We also investigated $G_P$ as a function of $P$ and $\phi$. With increasing $P$, $G_P$ increases over 1 order of magnitude as a power-law $G_P \sim P^{2.8}$, which is quantitatively consistent with colloidal gels assembled by depletion attractions alone.[11] As $\phi$ increases, $G_P$ increases over 2 orders of magnitude as a power-law $G_P \sim \phi^{4.1}$. Shih et al. suggested a scaling behavior relating macroscopic rheological properties to microstructures:[18] by assuming the gel network is composed of aggregated clusters, the scaling behavior of $G_P$ with $\phi$ provides the gel structural information in terms of the cluster fractal dimension,[18] $d_f$

$$G_P \sim \phi^x, \; x = \frac{1}{3 - d_f} \quad (12)$$

$$\gamma_L \sim \phi^y, \; y = \frac{1}{3 - d_f} \quad (13)$$

To conduct the scaling analysis, we measured the strain at the limit of linearity $\gamma_L$, as shown in Figure 4e, as a function of $\phi$



DOI: 10.1021/acs.langmuir.9b00596
Langmuir 2019, 35, 9464−9473

shown in Figure 4f. The calculation using eqs 12 and 13 gives $d_f$ = 2.76 and 2.5, respectively. We note that these are independent estimates of the fractal dimension and their close values (differing only by 10%) lend support to a fractal dimension in the range of 2.5−2.76. Moreover, the estimated fractal dimensions indicate formation of dense clusters. Interestingly, forming compact clusters requires multiple collisions to overcome an energetic barrier,[45] which is consistent with our interaction potential that also shows an energetic barrier in Figure 2c. Additionally, the positive correlation between $\gamma_L$ and $\phi$ suggests the elasticity is determined by the intercluster links,[18] which supports recent work by Whitaker et al. investigating depletion gel elasticity.[46]

**Effect of Droplet Size.** The microstructure of our gel shown in Figure 1c is consistent with the prediction from the mode-coupling theory (MCT) where the attractive glass line penetrates into the spinodal regime and the gelation is through an arrested phase separation.[47,48] To further compare to MCT, we probed the system properties as a function of droplet size (Figure 5). We found that gelation only occurs for droplets

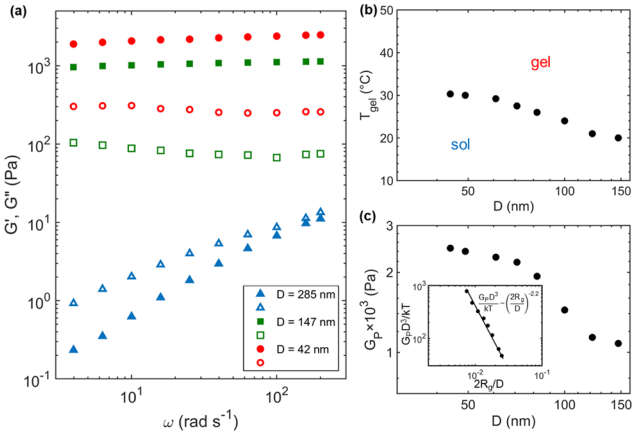


**Figure 5.** Effect of droplet diameter, $D$, on the nanoemulsion properties. Nanoemulsions of PDMS droplets with a volume fraction $\phi$ = 0.30 suspended in a continuous phase with PEGMA with a volume fraction $P$ = 0.33. (a) Linear viscoelasticity ($G'$: closed symbols, $G''$: open symbols) of the nanoemulsion with different $D$ at $T = T_{gel}$ + 25 °C. No gelation was observed across the experimental temperature window for $D$ > 150 nm. Within the gelation regime ($D$ < 150 nm), stronger gels are obtained for smaller $D$. Additionally, $G''$ of the gel shows a broad minimum at moderate angular frequencies, which is reminiscent of glassy dynamics indicating a transition from $\alpha$- to $\beta$-relaxation. (b) Gelation temperature, $T_{gel}$, as a function of $D$. For smaller $D$, a higher temperature is required to induce gelation. (c) Plateau modulus, $G_P$, as a function of $D$. The inset shows the normalized plateau modulus, $G_PD^3/kT$, as a function of normalized PEGMA depletion length scale, $2R_g/D$, where $R_g$ is the radius of gyration of PEGMA. The result shows a power-law behavior with an exponent = −2.2, consistent with predictions of mode-coupling theory (MCT).

with $D$ < 150 nm and a stronger gel was obtained as $D$ decreased, as shown in Figure 5a,c. We also observed a broad minimum in $G''$ in Figure 5a, which is reminiscent of glassy dynamics.[9,45] Within the gelation regime, $T_{gel}$ decreases with $D$, as shown in Figure 5b, which is consistent with MCT where gelation is more easily induced with larger $D$.[48] Inspired by MCT, we then expect a power law scaling of the normalized plateau modulus $G_PD^3/kT$ with $2R_g/D$ where $R_g$ = 0.55 nm is the radius of gyration of PEGMA. The resulting figure in Figure 5c shows that $G_PD^3/kT$ exhibits a power law behavior with $2R_g/D$ with an exponent of −2.2, which is in good agreement with the MCT prediction of −2.0.[48] Overall, the analyses show that the properties of our model nanoemulsion are in good agreement with theoretical studies and predictions can be made about the expected behavior of this platform system.

**Robustness of the Gelling Platform.** Finally, we investigated the gelling mechanism across a wide range of component chemistries (Figure 6). We first prepared nanoemulsions with PEG-based oligomers of different moieties, as shown in Figure 6a. Gelation was induced with all amphiphilic oligomers, and the less hydrophobic PEG results in higher $T_{gel}$ and smaller $G_P$. No gelation was observed with nonmodified PEG. The observation from oligomer chemistry supports our proposed mechanism where the dehydration of amphiphilic oligomers triggers the ionic surfactant displacement. We then prepared nanoemulsions with different types of surfactants, as shown in Figure 6b. Gelation was induced for all ionic surfactants, whereas no sol−gel transition was observed for the nonionic surfactant (Tween 20). This result highlights the importance of length scale, $\delta$, of each interaction in the gelling mechanism where $\delta_{PEGMA} \approx \delta_{electrosatic} \approx 1$ nm and $\delta_{Tween\ 20} \approx$ 3−4 nm.[49,50] Within the experimental window, nondisplaced Tween 20 provides a strong steric repulsion and prevents the system from gelling. Finally, we prepared the dispersion with solid polystyrene (PS) nanoparticles, as shown in Figure 6c, where the colloidal stability is provided by SDS adsorbed on the surface.[5] Remarkably, we found that this hard-sphere suspension exhibits a gelling behavior, demonstrating that our gelling platform is generic for both liquid and solid nanocolloids that allow surfactant exchange on the nanocolloid surface. No gelation is observed in the absence of PEGMA. Additionally, no sol−gel transition was observed for the aqueous continuous phase, indicating the gelation does not result from the self-assembly or association of SDS and PEGMA. We also measured the transmittance of PEGMA solution with $P$ = 0.33 using UV−vis spectroscopy at a wavelength = 500 nm at elevated temperatures (Figure 6c inset). The transmittance remains at 100% across the experimental temperature window and no phase separation is observed, suggesting PEGMA stably stays in the water. We note that the gelation mechanism presented here is different from our prior work where the gelation is through polymer bridging via difunctional gelators.[5,6,12,51]

## ■ CONCLUSIONS

Overall, we presented a colloidal gelation platform whose microstructure and mechanical properties can be controlled easily and reliably using an external temperature source. We systematically investigated the gelation mechanism and confirmed that it is due to thermally triggered surfactant displacement, which reduces the interparticle repulsion. By understanding the mechanism, we applied simple models to construct the interparticle potential and explain trends in material behaviors. The mechanistic understanding of the gelation also allowed us to extend the platform to other surfactant and colloid chemistries (both droplets and solid nanoparticles). This platform offers a convenient way to assemble and control the properties of a variety of different nanoparticle gels and will be useful for engineering advanced soft materials.



DOI: 10.1021/acs.langmuir.9b00596
Langmuir 2019, 35, 9464−9473

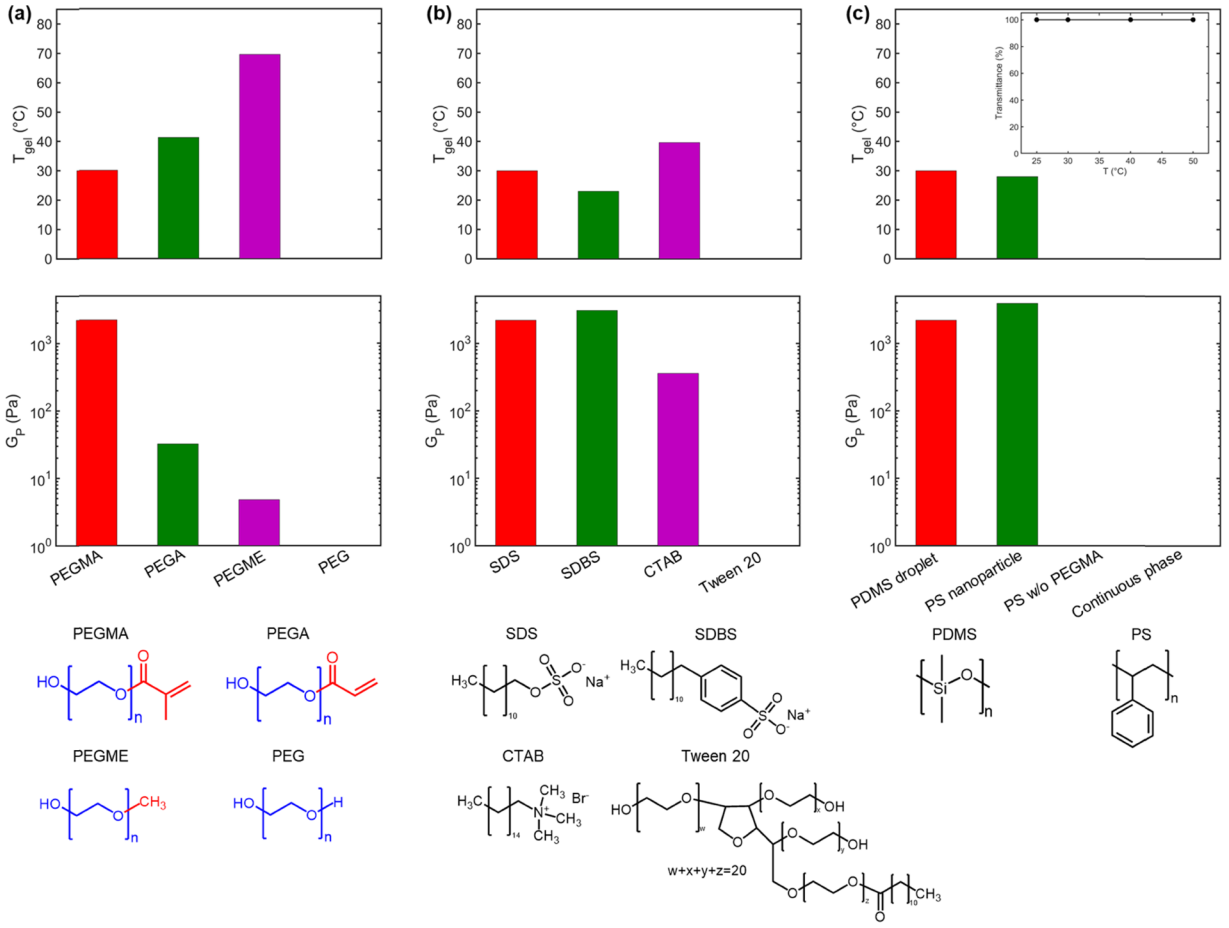


**Figure 6.** Gelation is robust across a wide range of component chemistries. Nanoemulsions here are composed of $\phi$ = 0.30 PDMS droplets of $D$ = 50 ± 1 nm in a continuous phase with $P$ = 0.33. The total concentration of surfactant is 0.175 M. (a) $T_{gel}$ and $G_P$ for various PEG-based oligomers with different moieties. The end groups are ordered in decreasing hydrophobicity, which results in a higher $T_{gel}$ and smaller $G_P$. For PEG with no end groups, gelation was not observed, consistent with our proposed mechanism where the surfactant displacement and the subsequent decrease in the repulsion are triggered by the dehydration of the functional end group (Figure 2a). (b) $T_{gel}$ and $G_P$ for various surfactants. Gelation was observed for all ionic surfactants, whereas no sol−gel transition was observed for the nonionic surfactant (Tween 20) across the experimental temperature window. (c) $T_{gel}$ and $G_P$ for two different nanoparticles. Gelation occurs for both liquid PDMS droplets and solid polystyrene (PS, $D$ = 58 nm and $\phi$ = 0.30) colloids. No gelation is observed with the absence of PEGMA. Additionally, no sol−gel transition was observed for the aqueous continuous phase, indicating the gelation does not result from the self-assembly or association of SDS and PEGMA. Inset: Transmittance of a pure PEGMA aqueous solution ($P$ = 0.33) as a function of temperature using UV−vis spectroscopy at a wavelength = 500 nm.

## ■ ASSOCIATED CONTENT

### Supporting Information

The Supporting Information is available free of charge on the ACS Publications website at DOI: 10.1021/acs.langmuir.9b00596.

Nanoemulsion synthesis and stability using dynamic light scattering, additional rheological characterization, ζ-potential measurements, ITC measurements and data analysis, estimation of droplet surface electrostatic potential (PDF)

## ■ AUTHOR INFORMATION


### Corresponding Author

*E-mail: pdoyle@mit.edu.

### ORCID

Li-Chiun Cheng: 0000-0001-5393-1982
Zachary M. Sherman: 0000-0001-9798-287X
Patrick S. Doyle: 0000-0003-2147-9172


### Notes

The authors declare no competing financial interest.

## ■ ACKNOWLEDGMENTS

This work was supported primarily by the MRSEC Program of the National Science Foundation under award number DMR—1419807 and in part by the National Science Foundation grant CMMI—1824297. We thank W. Salmon for discussions on confocal microscopy and C. A. P. Siepermann for discussions on isothermal titration calorimetry.

## ■ REFERENCES


(1) Wang, Q.; Wang, L.; Detamore, M. S.; Berkland, C. Biodegradable colloidal gels as moldable tissue engineering scaffolds. *Adv. Mater.* **2008**, *20*, 236−239.

(2) Wang, Q.; Wang, J.; Lu, Q.; Detamore, M. S.; Berkland, C. Injectable PLGA based colloidal gels for zero-order dexamethasone release in cranial defects. *Biomaterials* **2010**, *31*, 4980−4986.

(3) Dickinson, E. Stabilising emulsion-based colloidal structures with mixed food ingredients. *J. Sci. Food Agric.* **2013**, *93*, 710−721.




DOI: 10.1021/acs.langmuir.9b00596
*Langmuir* 2019, 35, 9464−9473

(4) Gibaud, T.; Mahmoudi, N.; Oberdisse, J.; Lindner, P.; Pedersen, J. S.; Oliveira, C. L. P.; Stradner, A.; Schurtenberger, P. New routes to food gels and glasses. *Faraday Discuss.* **2012**, *158*, 267−284.
(5) Cheng, L.-C.; Hsiao, L. C.; Doyle, P. S. Multiple particle tracking study of thermally-gelling nanoemulsions. *Soft Matter* **2017**, *13*, 6606−6619.
(6) Hsiao, L. C.; Badruddoza, A. Z. M.; Cheng, L.-C.; Doyle, P. S. 3D Printing of Self-Assembling Thermoresponsive Nanoemulsions into Hierarchical Mesostructured Hydrogels. *Soft Matter* **2017**, *13*, 921−929.
(7) Gan, T.; Zhang, Y.; Guan, Y. In Situ Gelation of P(NIPAM-HEMA) Microgel Dispersion and Its Applications as Injectable 3D Cell Scaffold. *Biomacromolecules* **2009**, *10*, 1410−1415.
(8) He, C.; Kim, S. W.; Lee, D. S. In situ gelling stimuli-sensitive block copolymer hydrogels for drug delivery. *J. Controlled Release* **2008**, *127*, 189−207.
(9) Zaccarelli, E. Colloidal gels: equilibrium and non-equilibrium routes. *J. Phys.: Condens. Matter* **2007**, *19*, 323101−323150.
(10) Lu, P. J.; Zaccarelli, E.; Ciulla, F.; Schofield, A. B.; Sciortino, F.; Weitz, D. A. Gelation of particles with short-range attraction. *Nature* **2008**, *453*, 499−503.
(11) Hsiao, L. C.; Newman, R. S.; Glotzer, S. C.; Solomon, M. J. Role of isostaticity and load-bearing microstructure in the elasticity of yielded colloidal gels. *Proc. Natl. Acad. Sci. U.S.A.* **2012**, *109*, 16029−16034.
(12) Cheng, L.-C.; Godfrin, P. D.; Swan, J. W.; Doyle, P. S. Thermal processing of thermogelling nanoemulsions as a route to tune material properties. *Soft Matter* **2018**, *14*, 5604−5614.
(13) Sherman, Z. M.; Ghosh, D.; Swan, J. W. Field-Directed Self-Assembly of Mutually Polarizable Nanoparticles. *Langmuir* **2018**, *34*, 7117−7134.
(14) Swan, J. W.; Vasquez, P. A.; Whitson, P. A.; Fincke, E. M.; Wakata, K.; Magnus, S. H.; Winne, F. D.; Barratt, M. R.; Agui, J. H.; Green, R. D.; et al. Multi-scale kinetics of a field-directed colloidal phase transition. *Proc. Natl. Acad. Sci. U.S.A.* **2012**, *109*, 16023−16028.
(15) Hoekstra, H.; Mewis, J.; Narayanan, T.; Vermant, J. Multi length scale analysis of the microstructure in sticky sphere dispersions during shear flow. *Langmuir* **2005**, *21*, 11017−11025.
(16) Eberle, A. P. R.; Castañeda-Priego, R.; Kim, J. M.; Wagner, N. J. Dynamical arrest, percolation, gelation, and glass formation in model nanoparticle dispersions with thermoreversible adhesive interactions. *Langmuir* **2012**, *28*, 1866−1878.
(17) Russel, W. B.; Saville, D. A.; Schowalter, W. R. *Colloidal Dispersions*; Cambridge University Press, 1989.
(18) Shih, W. H.; Shih, W. Y.; Kim, S.-I.; Liu, J.; Aksay, I. A. Scaling behavior of the elastic properties of colloidal gels. *Phys. Rev. A* **1990**, *42*, 4772−4779.
(19) Lindman, S.; Lynch, I.; Thulin, E.; Nilsson, H.; Dawson, K. A.; Linse, S. Systematic Investigation of the Thermodynamics of HSA Adsorption to N-tert-Butylacrylamide Copolymer Nanoparticles. Effects of Particle Size and Hydrophobicity. *Nano Lett.* **2007**, *7*, 914−920.
(20) Paula, S.; Sues, W.; Tuchtenhagen, J.; Blume, A. Thermodynamics of Micelle Formation as a Function of Temperature: A High Sensitivity Titration Calorimetry Study. *J. Phys. Chem. A* **1995**, *99*, 11742−11751.
(21) Gupta, A.; Eral, H. B.; Hatton, T. A.; Doyle, P. S. Nanoemulsions: formation, properties and applications. *Soft Matter* **2016**, *12*, 2826−2841.
(22) Helgeson, M. E. Colloidal behavior of nanoemulsions: Interactions, structure, and rheology. *Curr. Opin. Colloid Interface Sci.* **2016**, *25*, 39−50.
(23) Mason, T. G.; Wilking, J. N.; Meleson, K.; Chang, C. B.; Graves, S. M. Nanoemulsions: formation, structure, and physical properties. *J. Phys.: Condens. Matter* **2006**, *18*, R635−R666.
(24) Winter, H. H.; Chambon, F. Analysis of Linear Viscoelasticity of a Crosslinking Polymer at the Gel Point. *J. Rheol.* **1986**, *30*, 367−382.
(25) Chambon, F.; Winter, H. H. Linear Viscoelasticity at the Gel Point of a Crosslinking PDMS with Imbalanced Stoichiometry. *J. Rheol.* **1987**, *31*, 683−697.
(26) Winter, H. H. Gel Point. In *Encyclopedia of Polymer Science and Technology*; John Wiley & Sons, Inc., 2016; pp 1−15.
(27) Bhatia, S. R.; Mourchid, A. Gelation of Micellar Block Polyelectrolytes: Evidence of Glassy Behavior in an Attractive System. *Langmuir* **2002**, *18*, 6469−6472.
(28) Hiemenz, P. C.; Rajagopalan, R. *Principles of Colloid and Surface Chemistry*; CRC Press, 1997.
(29) Malmberg, C. G.; Maryott, A. A. Dielectric constant of water from 0 to 100 C. *J. Res. Natl. Bur. Stand.* **1956**, *56*, No. 1.
(30) Sengwa, R. J.; Kaur, K.; Chaudhary, R. Dielectric properties of low molecular weight poly(ethylene glycol)s. *Polym. Int.* **2000**, *49*, 599−608.
(31) Arnold, K.; Herrmann, A.; Pratsch, L.; Gawrisch, K. The dielectric properties of aqueous solutions of poly(ethylene glycol) and their influence on membrane structure. *Biochim. Biophys. Acta, Biomembr.* **1985**, *815*, 515−518.
(32) Ramakrishnan, S.; Gopalakrishnan, V.; Zukoski, C. F. Clustering and Mechanics in Dense Depletion and Thermal Gels. *Langmuir* **2005**, *21*, 9917−9925.
(33) Ramakrishnan, S.; Chen, Y.-L.; Schweizer, K. S.; Zukoski, C. F. Elasticity and clustering in concentrated depletion gels. *Phys. Rev. E* **2004**, *70*, No. 040401.
(34) Shah, S. A.; Chen, Y.-L.; Ramakrishnan, S.; Schweizer, K. S.; Zukoski, C. F. Microstructure of dense colloid−polymer suspensions and gels. *J. Phys.: Condens. Matter* **2003**, *15*, 4751−4778.
(35) Sherman, Z. M.; Swan, J. W. Dynamic, Directed Self-Assembly of Nanoparticles via Toggled Interactions. *ACS Nano* **2016**, *10*, 5260−5271.
(36) Sherman, Z. M.; Rosenthal, H.; Swan, J. W. Phase Separation Kinetics of Dynamically Self-Assembling Nanoparticles with Toggled Interactions. *Langmuir* **2018**, *34*, 1029−1041.
(37) Asakura, S.; Oosawa, F. Interaction between particles suspended in solutions of macromolecules. *J. Polym. Sci.* **1958**, *33*, 183−192.
(38) Lekkerkerker, H. N. W.; Tuinier, R. *Colloids and the Depletion Interaction*; Springer: Netherlands, 2011.
(39) Erramreddy, V. V.; Ghosh, S. Influence of emulsifier concentration on nanoemulsion gelation. *Langmuir* **2014**, *30*, 11062−11074.
(40) Petsev, D. N.; Denkov, N. D.; Kralchevsky, P. A. Flocculation of Deformable Emulsion Droplets. *J. Colloid Interface Sci.* **1995**, *176*, 201−213.
(41) Duplâtre, G.; Ferreira Marques, M. F.; da Graça Miguel, M. Size of Sodium Dodecyl Sulfate Micelles in Aqueous Solutions as Studied by Positron Annihilation Lifetime Spectroscopy. *J. Phys. Chem. A* **1996**, *100*, 16608−16612.
(42) Shah, S. S.; Jamroz, N. U.; Sharif, Q. M. Micellization parameters and electrostatic interactions in micellar solution of sodium dodecyl sulfate (SDS) at different temperatures. *Colloids Surf., A* **2001**, *178*, 199−206.
(43) Sainath, K.; Ghosh, P. Stabilization of Silicone Oil-in-Water Emulsions by Ionic Surfactant and Electrolytes: The Role of Adsorption and Electric Charge at the Interface. *Ind. Eng. Chem. Res.* **2013**, *52*, 15808−15816.
(44) Koh, A.; Gillies, G.; Gore, J.; Saunders, B. R. Flocculation and Coalescence of Oil-in-Water Poly(dimethylsiloxane) Emulsions. *J. Colloid Interface Sci.* **2000**, *227*, 390−397.
(45) Joshi, Y. M. Dynamics of Colloidal Glasses and Gels. *Annu. Rev. Chem. Biomol. Eng.* **2014**, *5*, 181−202.
(46) Whitaker, K. A.; Varga, Z.; Hsiao, L. C.; Solomon, M. J.; Swan, J. W.; Furst, E. M. Colloidal gel elasticity arises from the packing of locally glassy clusters. *Nat. Commun.* **2019**, *10*, No. 2237.
(47) Cardinaux, F.; Gibaud, T.; Stradner, A.; Schurtenberger, P. Interplay between spinodal decomposition and glass formation in proteins exhibiting short-range attractions. *Phys. Rev. Lett.* **2007**, *99*, 1−4.


DOI: 10.1021/acs.langmuir.9b00596
*Langmuir* 2019, 35, 9464−9473

(48) Chen, Y. L.; Schweizer, K. S. Microscopic theory of gelation and elasticity in polymer-particle suspensions. *J. Chem. Phys.* **2004**, *120*, 7212−7222.
(49) McClements, D. J.; Dickinson, E.; Dungan, S. R.; Kinsella, J. E.; Ma, J. G.; Povey, M. J. W. Effect of Emulsifier Type on the Crystallization Kinetics of Oil-in-Water Emulsions Containing a Mixture of Solid and Liquid Droplets. *J. Colloid Interface Sci.* **1993**, *160*, 293−297.
(50) Lee, H.; Venable, R. M.; MacKerell, A. D.; Pastor, R. W. Molecular dynamics studies of polyethylene oxide and polyethylene glycol: Hydrodynamic radius and shape anisotropy. *Biophys. J.* **2008**, *95*, 1590−1599.
(51) Helgeson, M. E.; Moran, S. E.; An, H. Z.; Doyle, P. S. Mesoporous organohydrogels from thermogelling photocrosslinkable nanoemulsions. *Nat. Mater.* **2012**, *11*, 344−352.



DOI: 10.1021/acs.langmuir.9b00596
*Langmuir* 2019, 35, 9464−9473